J. Fluid Mech. (2018), *vol.* 855, R1, doi:10.1017/jfm.2018.642

JFM RAPIDS
journals.cambridge.org/rapids

Upstream-travelling acoustic jet modes as a closure mechanism for screech

Daniel Edgington-Mitchell[1,†], Vincent Jaunet[2], Peter Jordan[2], Aaron Towne[3], Julio Soria[1] and Damon Honnery[1]

[1]Department of Mechanical and Aerospace Engineering, Monash University, VIC 3800, Australia

[2]Département Fluides, Thermique et Combustion, Institut Pprime, CNRS, Université de Poitiers, ENSMA, 86000 Poitiers, France

[3]Center for Turbulence Research, Stanford University, Stanford, CA 94305, USA

(Received 4 April 2018; revised 18 June 2018; accepted 2 August 2018)

Experimental evidence is provided to demonstrate that the upstream-travelling waves in two jets screeching in the A1 and A2 modes are not free-stream acoustic waves, but rather waves with support within the jet. Proper orthogonal decomposition is used to educe the coherent fluctuations associated with jet screech from a set of randomly sampled velocity fields. A streamwise Fourier transform is then used to isolate components with positive and negative phase speeds. The component with negative phase speed is shown, by comparison with a vortex-sheet model, to resemble the upstream-travelling jet wave first studied by Tam & Hu (*J. Fluid Mech.*, vol. 201, 1989, pp. 447–483). It is further demonstrated that screech tones are only observed over the frequency range where this upstream-travelling wave is propagative.

Key words: compressible flows, jet noise, shock waves

1. Introduction

Supersonic jets operating at off-design conditions are characterized by three distinct noise sources (Tam 1995): mixing noise (Jordan & Colonius 2013), broad-band shock associated noise (André, Castelain & Bailly 2013), and jet screech (Raman 1999). Turbulent wavepackets in the jet play a key role in all three mechanisms, while the shock structures resulting from the off-design operation of the jet are an integral part of the latter two. Screech was first described by Powell (1953*a*,*b*), who recognized that screech tones are the result of an aeroacoustic feedback process comprised of four stages: an upstream-travelling acoustic wave arrives at the nozzle lip, perturbing the near-nozzle shear layer. This perturbation grows through the Kelvin–Helmholtz instability, developing into a wavepacket as it convects downstream. The interaction

† Email address for correspondence: daniel.mitchell@monash.edu

of this wavepacket with shock structures resulting from off-design operation produces acoustic waves. These propagate back to the nozzle, closing the loop. As is typical of aeroacoustic resonance, the screech-tone frequency is selected both by the need to match the phase of the upstream and downstream disturbances, and to satisfy an amplitude criterion (the gain across the process must be equal to one). Screech is characterized by its discrete tonal nature, its strong directivity, and what is known as its 'staging' behaviour. As the pressure ratio (and thus the degree of underexpansion) is varied continuously, the screech tone initially changes in a similarly continuous manner. This change in tone is typically assumed to be due to gradual changes in the shock-cell spacing and convection velocity. However, at certain pressures, driven by the need to satisfy both the amplitude and gain criteria, the frequency of the screech tone changes discontinuously. In an axisymmetric jet, this jump in frequency is often accompanied by a change in the azimuthal structure of the screech mode; with increasing pressure ratio the flow undergoes: A1 and A2 (toroidal), B (precessing flapping), C (helical) and D (flapping) oscillations. While there have been attempts to produce frequency prediction models that can account for staging (Gao & Li 2010), or to explain the process in terms of changes in characteristic length scales of the flow (Edgington-Mitchell, Honnery & Soria 2015*b*), a clear phenomenological explanation has not been forthcoming.

This lack of a phenomenological explanation for jet screech is symptomatic of a broader lack of understanding regarding its underlying processes. The sound generation mechanisms are still a topic of some debate, though a consensus appears to be arising with respect to the shock-leakage model of Manning & Lele (2000), with both experimental (Edgington-Mitchell *et al.* 2014*b*) and numerical (Berland, Bogey & Bailly 2007) evidence steadily accruing. Even if it is accepted that sound is produced via shock leakage, it is not yet clear whether it is a single shock (Mercier, Castelain & Bailly 2017) or multiple shocks (Tam, Parrish & Viswanathan 2014) that are responsible for the tone production. Receptivity processes at the nozzle lip (Barone & Lele 2005) are highly sensitive to nozzle geometry (Raman 1997), and the short time scales involved render measurement difficult (Mitchell, Honnery & Soria 2012). Historically, the upstream propagation of the sound wave has received little attention; the propagation of a sound wave seems a relatively straightforward process compared to the other components of the feedback cycle. It is nonetheless this process that is the focus of this paper.

The typical description of jet screech suggests a closure mechanism wherein an acoustic wave, generated at downstream shock cells, propagates upstream through the hydrodynamic near field to the nozzle lip. Perhaps the only alternative theory to date was proposed by Shen & Tam (2002). It is well recognized that two screech modes can exist simultaneously, suggesting the potential for multiple possible closure mechanisms for the feedback loop. Shen & Tam (2002) hypothesized that in addition to the standard mechanism, the feedback loop could also be closed by an upstream-travelling acoustic jet mode. This mode (k_{TH}^{-}) was one of several that Tam & Hu (1989) identified in compressible jets, beyond the classical downstream-travelling Kelvin–Helmholtz mode. These k_{TH}^{-} waves have recently seen a resurgence of interest in the community, having provided phenomenological explanations for tones in subsonic jets (Schmidt *et al.* 2017; Towne *et al.* 2017), jet–plate (Bogey & Gojon 2017) and jet–edge interactions (Jordan *et al.* 2018). One of the earliest attempts to link k_{TH}^{-} waves to the feedback-loop closure was by provided by Tam & Ahuja (1990) for subsonic impinging jets:

NPR	M_j	Re	St	Mode
2.10	1.09	4.4×10^5	0.65	A1
2.25	1.14	4.7×10^5	0.63	A2

TABLE 1. Jet conditions.

> *'We would like to suggest an alternative proposal that the feedback is achieved by waves belonging to the intrinsic upstream-propagating neutral acoustic modes of the jet flow. These upstream-propagating acoustic wave modes, just as the instability wave modes, have well-defined radial and azimuthal structures. Also they are, as in the case of Kelvin–Helmholtz instability waves, supported and determined by the mean flow of the jet.'*

In this paper, non-time-resolved high-resolution particle image velocimetry is used to provide experimental evidence that this same upstream-travelling neutral acoustic mode is also responsible for closure of the feedback loop in jet screech. A triple decomposition based on proper orthogonal decomposition (POD) is used to reconstruct the oscillations of the flow associated with the screech tone. A Fourier transform is then used to separate the screech fluctuations into components with negative and positive phase velocities. A mode with negative phase velocity and support in the core of the jet is clearly visible in the data. The radial structure of this mode is extracted from the data, and compared to the upstream-travelling mode predicted by stability theory.

2. Experimental set-up

The planar PIV dataset was produced in the Laboratory for Turbulence Research in Aerospace and Combustion (LTRAC) gas jet facility (Weightman *et al.* 2017). The facility is optimized for PIV measurements and is not anechoic. Both cases considered here are of flow issuing from a purely converging nozzle of diameter $D = 15$ mm, with a radius of curvature of 67.15 mm, ending with a parallel section at the nozzle exit, and an external lip thickness of 5 mm. Particle images were obtained using a 12-bit Imperx B4820 camera, with a CCD array of 4872×3248 px, at an acquisition frequency of 2 Hz. The 600 nm diameter smoke particles (Mitchell, Honnery & Soria 2013) were illuminated in a 1 mm thick Nd : YAG laser light sheet by a pair of 6 ns pulses of approximately 160 mJ, separated by $\Delta t = 1$ µs. The multigrid algorithm of Soria (1996) was used to analyse the image pairs, with a final interrogation window size of $0.03D \times 0.03D$, a depth of field of $0.04D$, and a field of view of $5.7D \times 3.8D$. Two flow conditions are considered, falling in the A1 and A2 modes of jet screech, described in table 1. Only a single screech tone was evident in each case, with no simultaneous peaks or mode-switching observed. Here nozzle pressure ratio is defined as the ratio between the plenum and the ambient pressures $NPR = p_0/p_\infty$, while the ideally expanded Mach number M_j, Reynolds number $Re = U_j D_j/\nu$ and Strouhal number $St = fD_j/U_j$ are calculated based on isentropic expansion to ambient pressure, where U_j is the ideally-expanded velocity, D_j is the ideally-expanded equivalent jet diameter, ν is the kinematic viscosity and f is the screech frequency. The Strouhal number listed in table 1 is that of the fundamental screech tone measured by a G.R.A.S. type 46BE 1/4″ pre-amplified microphone in the far field.

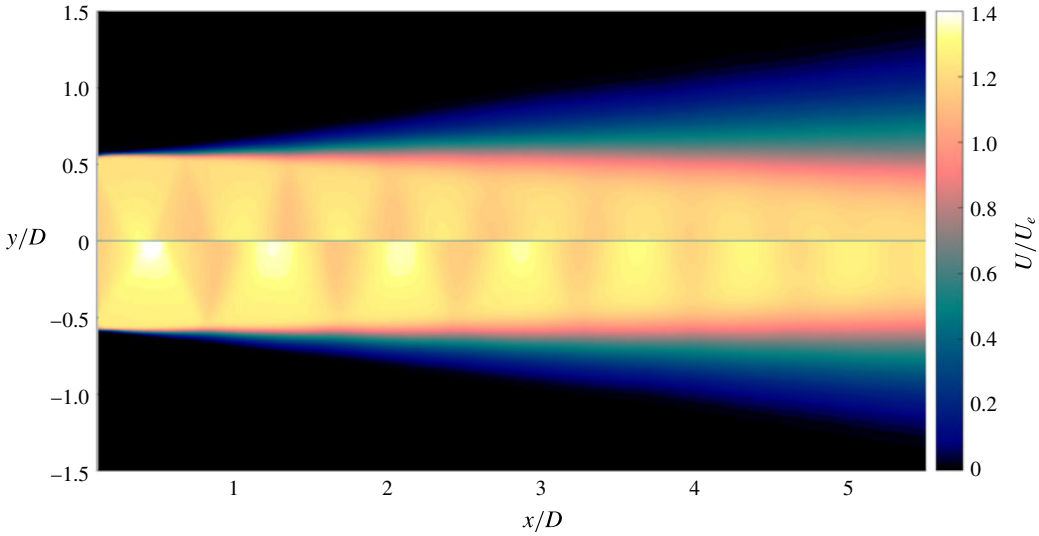

FIGURE 1. Mean axial velocity: (top) $NPR = 2.10$ and (bottom) $NPR = 2.25$.

3. Mean flows and decomposition

Contours of the mean axial velocity for the jets, averaged over 10 000 individual fields, are presented in figure 1. Both flow fields exhibit the typical shock-expansion pattern of underexpanded jets. The small difference in pressure ratio is sufficient to cause a moderate change in the spacing and strength of the shock cells.

To extract the fluctuations associated with the screech tone, the snapshot POD of Sirovich (1987) is applied. The spatial quasi-periodicity of screeching and impinging jets make them amenable to POD. The decomposition is performed only on the transverse velocity fluctuation, as this provides a clearer separation for the leading mode pair. Only key details of the approach are reproduced here. The autocovariance matrix is constructed from the velocity snapshots $\boldsymbol{R} = \boldsymbol{V}^{\mathrm{T}}\boldsymbol{V}$, and the solution of the eigenvalue problem $\boldsymbol{R}\boldsymbol{v} = \lambda\boldsymbol{v}$ yields the eigenvalues λ and eigenvectors $\boldsymbol{v}$ from which the spatial POD modes are constructed as:

$$\boldsymbol{\phi}_n(x, y) = \frac{\boldsymbol{V}\boldsymbol{v}_n(t)}{\|\boldsymbol{V}\boldsymbol{v}_n(t)\|}, \tag{3.1}$$

and the coefficients at each time t for each mode n can be expressed as:

$$\boldsymbol{a}_n(t) = \boldsymbol{v}_n(t)\|\boldsymbol{V}\boldsymbol{v}_n(t)\|. \tag{3.2}$$

Both jets are characterized by a leading pair of POD modes that are symmetric about the centreline, which at these pressure ratios is indicative of an $m = 0$ azimuthal mode; these modes are shown in figure 2. At first glance there appears to be almost no difference in modal structure between the two cases. Figure 3 indicates that the leading mode pair represents only a relatively small fraction of the total energy, but this is typical of high-Reynolds-number screeching jets (Edgington-Mitchell, Honnery & Soria 2015*a*). The Lissajous curves in figure 3, formed by plotting the mean radial distance to the snapshot coefficients, form a circle, indicating that modes 1 and 2

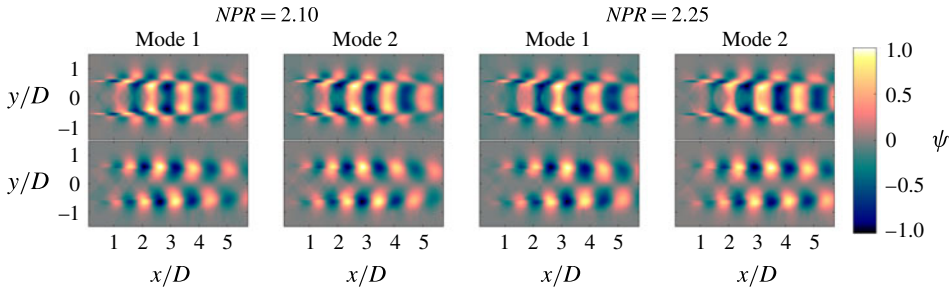

FIGURE 2. Axial u_c (above) and transverse v_c (below) components of proper orthogonal modes 1 and 2 for both cases. Each mode is individually normalized.

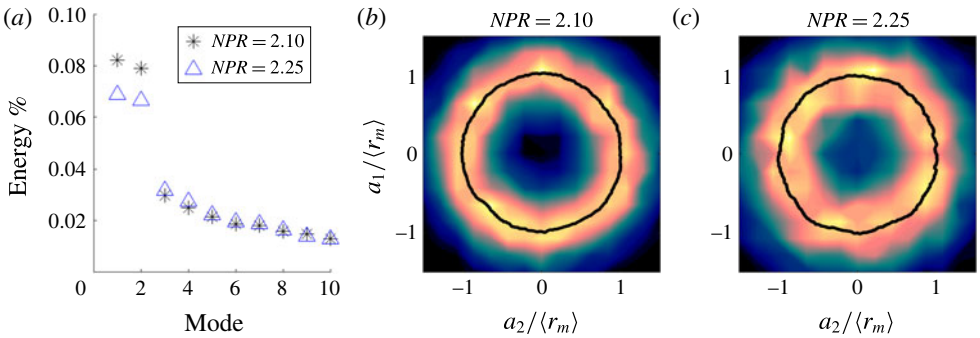

FIGURE 3. (*a*) Energy distribution amongst leading POD modes; (*b*,*c*) phase portrait of the leading two POD modes for each case, constructed from the eigenvectors associated with those modes, represented as a PDF.

represent a periodic phenomenon. Extensive prior experience with self-forcing flows of this kind demonstrates that it is reasonable to assume that the leading mode pair will represent the coherent structures associated with the aeroacoustic feedback process (Edgington-Mitchell, Honnery & Soria 2014*a*). The coherent fluctuations associated with these structures ($\boldsymbol{q}^c(x, y, t)$) can thus be extracted from the PIV data using the leading pair of POD modes:

$$\boldsymbol{q}^c(x, y, t) = \sum_{n=1}^{2} a_n(t)\boldsymbol{\phi}_n(x, y) = \mathrm{Re}(\boldsymbol{a}(t)\boldsymbol{\psi}(x, y)). \tag{3.3}$$

Since the mode pair represents a periodic phenomenon at the screech frequency ω_s, after Oberleithner *et al.* (2011) and Jaunet, Collin & Delville (2016) we define: $\boldsymbol{a} = a_1 - ia_2 = \hat{a}\mathrm{e}^{-\mathrm{i}\omega_s t}$ and $\boldsymbol{\psi} = \boldsymbol{\phi}_1 + \mathrm{i}\boldsymbol{\phi}_2$. On this basis, with the application of a streamwise Fourier transform, the coherent fluctuations can be represented:

$$\boldsymbol{q}^c(x, y, t) = \hat{a}\mathrm{e}^{-\mathrm{i}\omega_s t}\sum_k \hat{\boldsymbol{q}}_k^c(y)\mathrm{e}^{\mathrm{i}kx}. \tag{3.4}$$

Here the temporal Fourier coefficients have been constructed directly from the complex POD mode pair $\boldsymbol{\psi}$, such that:

$$\hat{\boldsymbol{q}}_k^c(y) = \sum_x \boldsymbol{\psi}(x, y)\mathrm{e}^{-\mathrm{i}kx}. \tag{3.5}$$

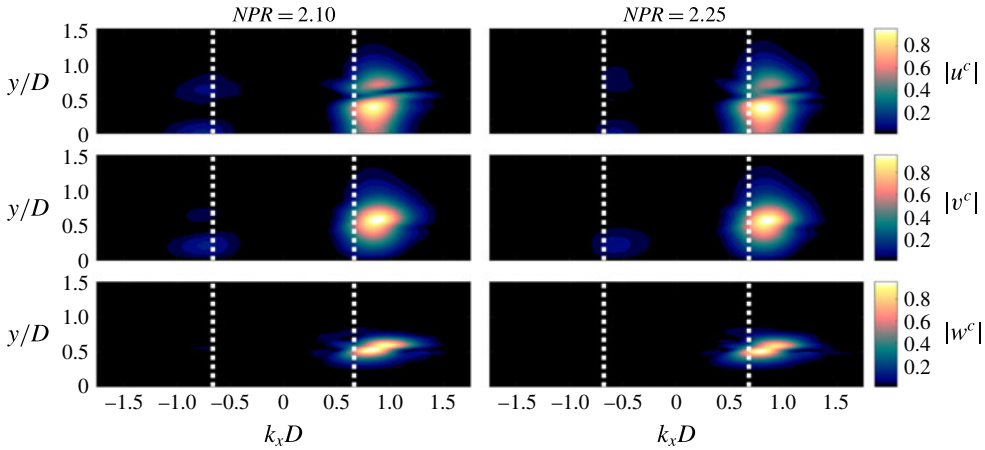

FIGURE 4. Axial, transverse and vortical wavenumber spectra at the screech frequency. Dotted vertical lines denote the speed of sound in the upstream and downstream directions. Negative wavenumbers correspond to phase velocities in the upstream direction, positive wavenumbers correspond to waves travelling downstream.

4. The upstream-travelling k_{TH}^- mode

4.1. *Experimental evidence*

The amplitude of (3.5), for $\boldsymbol{q}^c = [\boldsymbol{u}^c, \boldsymbol{v}^c, \boldsymbol{\omega}_z^c]$ is plotted as a function of spatial wavenumber k_x in figure 4. The sign of k_x determines the sign of the phase velocity. We use the sign of the phase velocity as a proxy for the sign of the group velocity, which determines the direction of energy propagation, i.e. the direction the wave travels. This is justified by the fact that all of the waves in question, i.e. the Kelvin–Helmholtz waves, free-stream acoustic waves and upstream-travelling k_{TH}^- waves, have phase and group velocities of the same sign in supersonic jets (Towne *et al.* 2017).

The vertical white lines indicate wavenumbers associated with the upstream and downstream speed of sound (a_∞) respectively, calculated as $k_x = \pm\omega_s/2\pi \times a_\infty$. As expected, the majority of the fluctuating energy is associated with a downstream-travelling wave moving at approximately $U_c \approx 0.7U_j$, with peak amplitudes in the shear layer of the jet. However, there is evidence of a component with negative phase speed for both the A1 and A2 cases, with a radial structure quite different from that of the downstream-travelling waves, and a propagation velocity close to the speed of sound. The minimal vorticity fluctuation and acoustic wavespeed indicate that this is an acoustic rather than hydrodynamic perturbation.

The upstream-travelling wave is isolated by bandpass filtering the space-time decomposed data (as per (3.5)) about the negative speed of sound, with a bandwidth of $\Delta k_x = 0.45D$. The downstream component is also isolated, by high-pass filtering for $k_x \geqslant 0$. A reconstruction of the screech-tone phase cycle for both the upstream-travelling and downstream-travelling components can be viewed in Supplementary Movies 1 and 2 available at https://doi.org/10.1017/jfm.2018.642.

The amplitudes of the components with positive and negative phase speed are presented in figure 5. The downstream fluctuations are dominated by the large-scale structures that develop from the Kelvin–Helmholtz instability, and the amplitude distribution here is consistent with the growth, saturation and decay of these

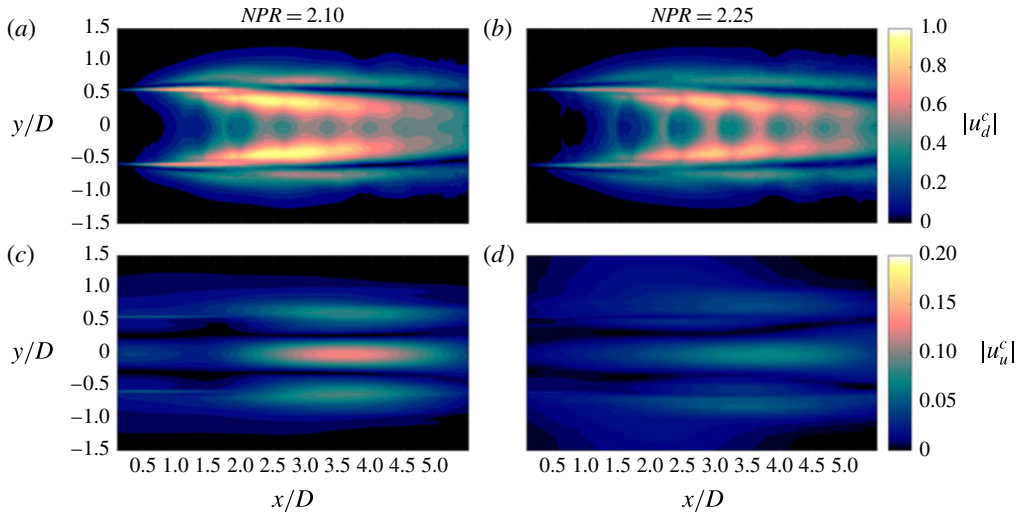

FIGURE 5. Amplitude distributions for downstream (u_d^c) and upstream (u_u^c) travelling components of the coherent axial velocity fluctuations determined from the leading POD mode pair. All values normalized by the maximum of u_d^c.

wavepackets. For both cases, the spatial distribution of the downstream-travelling fluctuations is very similar: the majority of the fluctuation takes place in the shear layer, reaching a maximum around the fourth or fifth shock cell. Modulation of the large-scale structures by the shocks is evident even at this relatively low pressure ratio (Tan *et al.* 2017). The amplitude of the fluctuations associated with the negative phase-speed component presents a very different spatial distribution with much lower peak amplitude. For both cases, the amplitude peaks in the jet core, with a maximum occurring farther downstream than for the Kelvin–Helmholtz structures. The only notable difference between the two cases is evident in the radial profile at $x/D = 2.5$, plotted in figure 6; while the peak amplitudes are higher for $NPR = 2.10$, the radial amplitude decay begins slightly farther from the centreline for $NPR = 2.25$. Figure 6 also presents axial plots of transversely integrated amplitude (to account for axisymmetry). It is clear that the overall specific energy associated with the upstream mode is quite similar for both cases. For both jets there is an axial amplitude envelope, peaking between the third and fourth shock reflection points for $NPR = 2.25$ and at the fifth shock cell for $NPR = 2.10$.

Thus for both the A1 and A2 stages, the following statement may be made: there is a mode with negative phase speed and radial support in both the core and the shear layer. This mode has a phase velocity nearly equal to the speed of sound, and does not appear to be hydrodynamic in nature. The signature of this mode appears for both the A1 and A2 stages of jet screech.

4.2. *Predictions from theory*

To verify whether the upstream-travelling mode is that originally identified by Tam & Hu (1989), we use a cylindrical vortex sheet to model the upstream-travelling waves. The dispersion relation was first derived by Lessen, Fox & Zien (1965) and has been used to study stability behaviour of a variety of subsonic and supersonic jets, for instance by Michalke (1970), Towne *et al.* (2017), Jordan *et al.* (2018), and of course

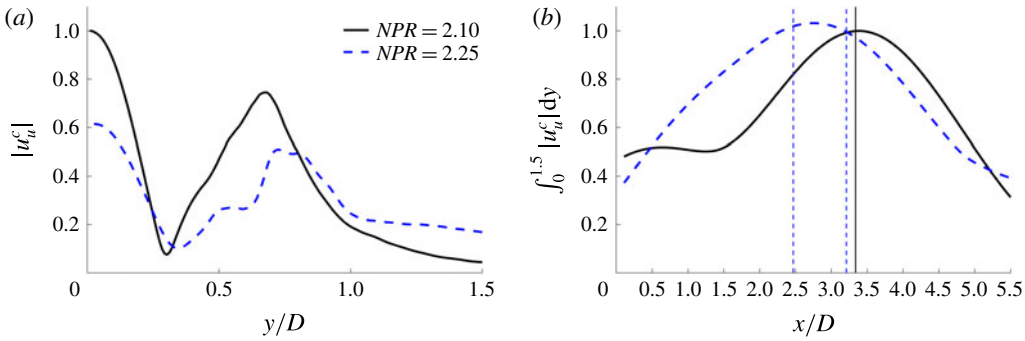

FIGURE 6. (*a*) Radial profile of the upstream-travelling mode amplitude, taken at $x/D = 2.5$, normalized by the maximum value of the $NPR = 2.10$ mode. (*b*) Axial profile of the transverse integral of the upstream-travelling mode amplitude. Vertical lines in (*b*) indicate the location of shock reflection points: solid black line = fifth shock reflection point for $NPR = 2.10$, dashed blue lines = third and fourth shock reflection points for $NPR = 2.25$.

in the original work of Tam & Hu (1989). It can be written:

$$\frac{1}{(\omega - kM)^2} + \frac{1}{T}\frac{\mathrm{I}_m\left(\frac{\gamma_i}{2}\right)\left[\frac{\gamma_o}{2}\mathrm{K}_{m-1}\left(\frac{\gamma_o}{2}\right) + m\mathrm{K}_m\left(\frac{\gamma_o}{2}\right)\right]}{\mathrm{K}_m\left(\frac{\gamma_o}{2}\right)\left[\frac{\gamma_i}{2}\mathrm{I}_{m-1}\left(\frac{\gamma_i}{2}\right) + m\mathrm{I}_m\left(\frac{\gamma_i}{2}\right)\right]} = 0. \tag{4.1}$$

The spatial eigenvalues of the vortex sheet are given by the roots $k(\omega)$ for real values of ω. These are found using Fletcher's version of the Levenberg–Marquardt algorithm for minimizing a sum of squares of the equation residuals. For a given eigenvalue $k(\omega)$, the streamwise velocity of the corresponding eigenfunction is

$$u_x(r) = \begin{cases} -\dfrac{k\mathrm{I}_m(\gamma_i r)}{Mk - \omega} & \text{for } 0 \leqslant r \leqslant 0.5 \\ -\dfrac{k\mathrm{K}_m(\gamma_o r)}{Mk - \omega} & \text{for } r \geqslant 0.5. \end{cases} \tag{4.2}$$

I_m and K_m are mth-order, modified Bessel functions of the first and second kind, respectively,

$$\gamma_i = \sqrt{k^2 - (\omega - Mk)^2}, \quad \text{and} \quad \gamma_o = \sqrt{k^2 - \omega^2}. \tag{4.3a,b}$$

The branch cut of the square root is chosen such that the real parts of $\gamma_{i,o}$ are positive.

For each azimuthal wavenumber m, there exists a countably infinite set of solutions $n = 1, 2, 3, \ldots$ that are ordered according to their effective radial wavenumber n (Towne *et al.* 2017). Figure 7 shows the dispersion relations associated with upstream- and downstream-travelling waves of azimuthal-radial orders (0, 1) and (0, 2). The red cross-hairs identify the eigenvalue selected for comparison with the measured amplitude of the upstream-travelling component u_u^c, also shown in figure 7(*b*). The agreement between model and experiment is remarkable, given that a vortex-sheet model is being used to compare with a non-parallel, nonlinear, shock-containing jet. The inner structure of the wave is captured with excellent accuracy by the vortex sheet, and the amplitude jump across the shear layer is captured at least qualitatively.

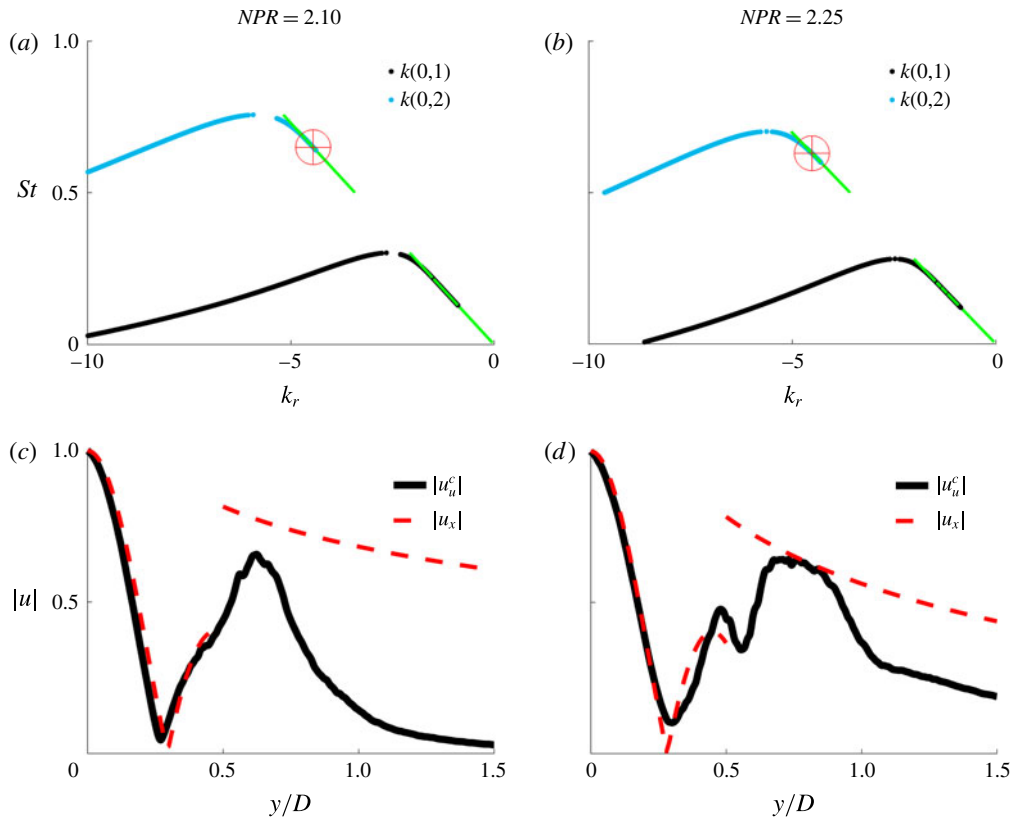

FIGURE 7. (*a*,*c*) Cylindrical vortex-sheet dispersion relations for waves $k(m, n)$. The green line shows dispersion relations for upstream-travelling free-stream sound waves. The red cross-hairs identify the eigenvalue considered for comparison with the experimental data. (*b*,*d*) Comparison of an experimentally educed $|u_u^c|$ as per figure 5, extracted at an axial position of $x/D = 3.0$, with the vortex-sheet eigenfunction $|u_x|$ associated with the selected eigenvalue. Cartesian coordinates are used for the axis, with the radial coordinate in the vortex-sheet model transformed such that $y = r$.

The agreement in the inner region suggests that the upstream-travelling wave may indeed be a k_{TH}^- wave; however, the continuous branch of the vortex-sheet eigenvalue spectrum (representing free-stream acoustic waves) is characterized by modes with similar eigenfunctions. Demonstrating that the k_{TH}^- mode is the upstream component of resonance requires a consideration of the frequencies over which this mode is propagative. Figure 8 presents acoustic data acquired in the SUCRE (SUpersoniC REsonance) semi-anechoic jet facility at Institut PPRIME. Overlaid on the acoustic spectra are lines indicating the cut-on and cutoff frequencies for the $(m, n) = (0, 2)$ k_{TH}^- mode as a function of Mach number, determined from the vortex-sheet analysis. In the region bounded by these curves, the k_{TH}^- mode is propagative; outside this range, the mode is evanescent. All of the observed tones for both the A1 and A2 modes fall within the frequency range where the mode is propagative; no resonance involving axisymmetric tones is observed outside of this range. This strongly supports the hypothesis that it is the k_{TH}^- mode observed in the experimental data, and that this mode is responsible for closing the resonance loop. Shen & Tam (2002) suggested

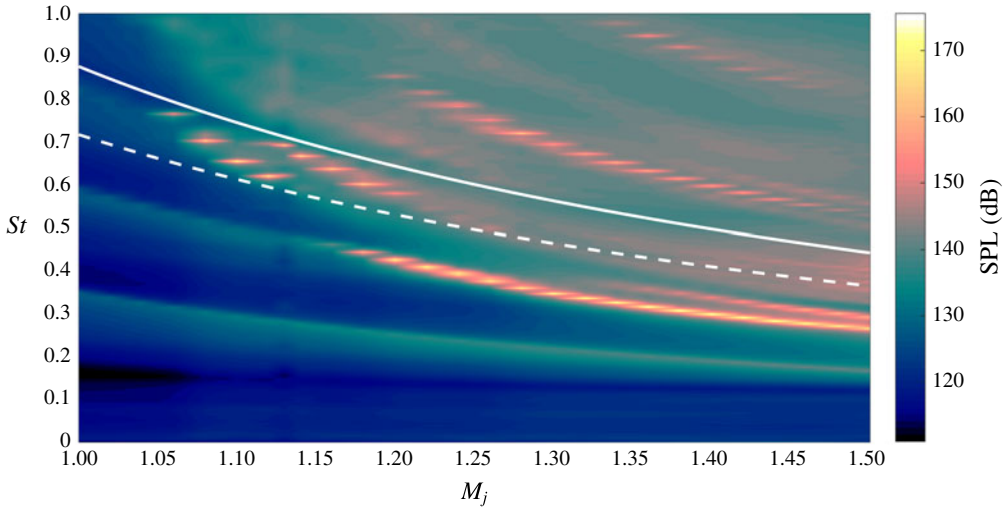

FIGURE 8. Contours of sound pressure level (SPL) as a function of jet operating conditions. The dashed white line indicates the cut-on frequency for the $(m, n) = (0, 2)$ k_{TH}^{-} mode at a given Mach number; below this frequency the mode is evanescent. The solid white line indicates the cutoff frequency; above this frequency the mode is evanescent. The region bounded by the curves thus represents the range of M–St space where the k_{TH}^{-} mode is propagative.

that the A1 and A2 modes were closed by different mechanisms: free-stream acoustic waves for the A1 mode, and the k_{TH}^{-} mode identified by Tam & Hu (1989) for the A2 mode. However the radial structures in figure 7 and the cut-on/cutoff behaviour observed in figure 8 suggest the same mechanism is at work for both the A1 and A2 screech stages.

5. Conclusion

Experimental evidence has been provided to suggest that the upstream-travelling wave that closes the A1 and A2 modes of jet screech is not a free-stream acoustic wave. Rather it is a discrete acoustic jet mode with support in both the jet core and shear layer. The experimental data has been supported by comparison with a vortex-sheet model, demonstrating close agreement between the measured and modelled radial structures of the modes. It has further been demonstrated that resonance only occurs for the frequency–Mach number range where the k_{TH}^{-} is propagative. In contrast to the original suggestion of Shen & Tam (2002), we see evidence that the upstream propagation is the same neutrally-stable acoustic mode for both the A1 and A2 jet screech modes. That the upstream-travelling mode is an intrinsic mode of the jet represents a significant change in the understanding of the screech phenomena, and will hopefully pave the way to a full phenomenological explanation.

Acknowledgements

This research was supported by the Australian Research Council through the Discovery Project scheme. The authors would also like to acknowledge the valuable contributions of Professor K. Oberleithner and Professor A. Cavalieri.

Supplementary movies

Supplementary movies are available at https://doi.org/10.1017/jfm.2018.642.

References

André, B., Castelain, T. & Bailly, C. 2013 Broadband shock-associated noise in screeching and non-screeching underexpanded supersonic jets. *AIAA J.* **51** (3), 665–673.

Barone, M. F. & Lele, S. K. 2005 Receptivity of the compressible mixing layer. *J. Fluid Mech.* **540**, 301–335.

Berland, J., Bogey, C. & Bailly, C. 2007 Numerical study of screech generation in a planar supersonic jet. *Phys. Fluids* **19** (7), 075105.

Bogey, C. & Gojon, R. 2017 Feedback loop and upwind-propagating waves in ideally expanded supersonic impinging round jets. *J. Fluid Mech.* **823**, 562–591.

Edgington-Mitchell, D., Honnery, D. R. & Soria, J. 2014*a* The underexpanded jet Mach disk and its associated shear layer. *Phys. Fluids* **26** (9), 096101.

Edgington-Mitchell, D., Honnery, D. R. & Soria, J. 2015*a* Multimodal instability in the weakly underexpanded elliptic jet. *AIAA J.* **53** (9), 2739–2749.

Edgington-Mitchell, D., Honnery, D. R. & Soria, J. 2015*b* Staging behaviour in screeching elliptical jets. *Intl J. Aeroacoust.* **14** (7), 1005–1024.

Edgington-Mitchell, D., Oberleithner, K., Honnery, D. R. & Soria, J. 2014*b* Coherent structure and sound production in the helical mode of a screeching axisymmetric jet. *J. Fluid Mech.* **748**, 822–847.

Gao, J. & Li, X. 2010 A multi-mode screech frequency prediction formula for circular supersonic jets. *J. Acoust. Soc. Am.* **127** (3), 1251–1257.

Jaunet, V., Collin, E. & Delville, J. 2016 POD-Galerkin advection model for convective flow: application to a flapping rectangular supersonic jet. *Exp. Fluids* **57** (5), 84.

Jordan, P. & Colonius, T. 2013 Wave packets and turbulent jet noise. *Annu. Rev. Fluid Mech.* **45**, 173–195.

Jordan, P., Jaunet, V., Towne, A., Cavalieri, A. V. G., Colonius, T., Schmidt, O. & Agarwal, A. 2018 Jet-flap interaction tones. *J. Fluid Mech.* **853**, 333–358.

Lessen, M., Fox, J. & Zien, H. 1965 On the inviscid stability of the laminar mixing of two parallel streams of a compressible fluid. *J. Fluid Mech.* **23** (2), 355–367.

Manning, T. & Lele, S. 2000 A numerical investigation of sound generation in supersonic jet screech. In *21st AIAA Aeroacoustics Conference, Lahaina, HI*. American Institute of Aeronautics and Astronautics.

Mercier, B., Castelain, T. & Bailly, C. 2017 Experimental characterisation of the screech feedback loop in underexpanded round jets. *J. Fluid Mech.* **824**, 202–229.

Michalke, A. 1970 A note on the spatial jet-instability of the compressible cylindrical vortex sheet. *Deutsche Forschungs-und Versuchsanstalt für Luft-und Raumfahrt*, eV, DLR FB 70-57.

Mitchell, D. M., Honnery, D. R. & Soria, J. 2012 The visualization of the acoustic feedback loop in impinging underexpanded supersonic jet flows using ultra-high frame rate schlieren. *J. Vis.* **15** (4), 333–341.

Mitchell, D. M., Honnery, D. R. & Soria, J. 2013 Near-field structure of underexpanded elliptic jets. *Exp. Fluids* **54** (7), 1578.

Oberleithner, K., Sieber, M., Nayeri, C., Paschereit, C., Petz, C., Hege, H.-C., Noack, B. & Wygnanski, I. 2011 Three-dimensional coherent structures in a swirling jet undergoing vortex breakdown: stability analysis and empirical mode construction. *J. Fluid Mech.* **679**, 383–414.

Powell, A. 1953*a* The noise of choked jets. *J. Acoust. Soc. Am.* **25** (3), 385–389.

Powell, A. 1953*b* On the mechanism of choked jet noise. *Proc. Phys. Soc.* B **66** (12), 1039.

Raman, G. 1997 Cessation of screech in underexpanded jets. *J. Fluid Mech.* **336**, 69–90.

Raman, G. 1999 Supersonic jet screech: half-century from Powell to the present. *J. Sound Vib.* **225** (3), 543–571.

SCHMIDT, O. T., TOWNE, A., COLONIUS, T., CAVALIERI, A. V., JORDAN, P. & BRÈS, G. A. 2017 Wavepackets and trapped acoustic modes in a turbulent jet: coherent structure eduction and global stability. *J. Fluid Mech.* **825**, 1153–1181.

SHEN, H. & TAM, C. K. 2002 Three-dimensional numerical simulation of the jet screech phenomenon. *AIAA J.* **40** (1), 33–41.

SIROVICH, L. 1987 Turbulence and the dynamics of coherent structures. i. Coherent structures. *Q. Appl. Maths* **45** (3), 561–571.

SORIA, J. 1996 An investigation of the near wake of a circular cylinder using a video-based digital cross-correlation particle image velocimetry technique. *Exp. Therm. Fluid Sci.* **12**, 221–233.

TAM, C. K. 1995 Supersonic jet noise. *Annu. Rev. Fluid Mech.* **27** (1), 17–43.

TAM, C. K. & AHUJA, K. 1990 Theoretical model of discrete tone generation by impinging jets. *J. Fluid Mech.* **214**, 67–87.

TAM, C. K. & HU, F. Q. 1989 On the three families of instability waves of high-speed jets. *J. Fluid Mech.* **201**, 447–483.

TAM, C. K., PARRISH, S. A. & VISWANATHAN, K. 2014 Harmonics of jet screech tones. *AIAA J.* **52** (11), 2471–2479.

TAN, D., SORIA, J., HONNERY, D. & EDGINGTON-MITCHELL, D. 2017 Novel method for investigating broadband velocity fluctuations in axisymmetric screeching jets. *AIAA J.* **55** (7), 2321–2334.

TOWNE, A., CAVALIERI, A. V., JORDAN, P., COLONIUS, T., SCHMIDT, O., JAUNET, V. & BRÈS, G. A. 2017 Acoustic resonance in the potential core of subsonic jets. *J. Fluid Mech.* **825**, 1113–1152.

WEIGHTMAN, J. L., AMILI, O., HONNERY, D., SORIA, J. & EDGINGTON-MITCHELL, D. 2017 An explanation for the phase lag in supersonic jet impingement. *J. Fluid Mech.* **815**, R1.